Chemical Engineering Journal 237 (2014) 336–343

Contents lists available at ScienceDirect

Chemical Engineering Journal

journal homepage: www.elsevier.com/locate/cej

Au nanoparticles decorated Kapok fiber by a facile noncovalent approach for efficient catalytic decoloration of Congo Red and hydrogen production

Wenbo Wang [a], Fangfang Wang [a,b], Yuru Kang [a], Aiqin Wang [a,*]

[a] Center of Eco-Material and Green Chemistry, Lanzhou Institute of Chemical Physics, Chinese Academy of Sciences, Lanzhou 730000, PR China
[b] School of Petrochemical Engineering, Lanzhou University of Technology, Lanzhou 730050, PR China

HIGHLIGHTS

- Au-NPs were immobilized on natural tubular Kappa fiber for catalytic applications.
- The preparation process is simple, mild, efficient and eco-friendly.
- The eco-friendly nanocomposite can rapidly catalyze the reduction of Congo Red dye.
- Hydrogen was simultaneously produced along with the catalytic reduction of dye.
- The nanocomposite can be used to treat dye wastewater and produce hydrogen.

GRAPHICAL ABSTRACT

AuNPs were immobilized on natural tubular Kappa fiber by a facile and green approach to derive new eco-friendly catalyst for efficient decoloration of CR dye and hydrogen production.

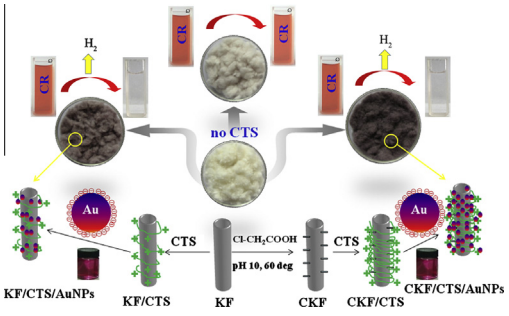

ARTICLE INFO

Article history:
Received 7 June 2013
Received in revised form 9 October 2013
Accepted 15 October 2013
Available online 24 October 2013

Keywords:
Kapok fiber
Gold nanoparticles
Nanocomposite
Catalytic reduction
Hydrogen production

ABSTRACT

A facile and eco-friendly noncovalent self-assembly approach was employed to immobilize Au nanoparticles (AuNPs) onto a natural tubular Kapok fiber (KF) and used for the catalytic reducing decoloration of Congo Red (CR) dye and simultaneous hydrogen production. AuNPs fail to be directly attached on KF or carboxylated KF (CKF), but the introduction of chitosan (CTS) as a "bridge" led to the stable immobilization of AuNPs on KF or CKF with a well-dispersed distribution, as shown by UV–*vis*, XRD, SEM and TEM analyses. The resultant KF (or CKF)/CTS/AuNPs nanocomposites show excellent catalytic activity and stability for the catalytic reducing decoloration of CR dye, and the color of CR solution can be rapidly faded within 3 min at the low catalyst dosage of 0.3 g/L. The catalytic activity of the nanocomposite can be maintained after being treated with sonication or 1 mol/L acid for 20 min. Along with the catalytic decoloration of CR, hydrogen was simultaneously produced and can be collected as a clean green fuel, and the maximum yield of hydrogen reaches 430 mL/L (CR solution, 20 mg/L). Thus, the nanocomposite can be used as a catalyst to decolor dye wastewater and produce hydrogen by one-step process. Moreover, the reported strategy follows the sustainable development idea of "from nature, for nature, into the nature" and promotes the use of naturally renewable resources to produce promising and eco-friendly functional materials for various applications.

1. Introduction

Gold nanoparticles (AuNPs) have attracted considerable attentions in many frontier fields such as biomedicine [1,2], electronics

* Corresponding author. Tel.: +86 931 4968118; fax: +86 931 8277088.
E-mail address: aqwang@licp.cas.cn (A. Wang).

1385-8947/$ - see front matter © 2013 Elsevier B.V. All rights reserved.
http://dx.doi.org/10.1016/j.cej.2013.10.044

[3,4], sensing [5,6], smart materials [7,8], solar cell [9] and catalysis [10,11]. As the catalysts, AuNPs show excellent activity superior to the bulk metals due to their large surface area-to-volume ratio. However, AuNPs are prone to aggregate in solution due to their higher surface energy, which greatly decrease and even minimize their catalytic activity. To overcome this, AuNPs were immobilized on various nano-carriers, such as carbon nanotubes [12,13], graphene [14–16], nanofiber [17], cellulose [18,19], clay [20], nanospheres [21], mesostructure material [22], and TiO_2 nanotube arrays [23], to form nanocomposites with well dispersion of AuNPs, stable structure and desirable hybrid properties.

Of these, natural polymers have focused much attention due to their renewable, low cost, reactive and eco-friendly advantages [24,25]. Thus far, two main approaches were employed to fabricate natural polymer/AuNPs composites: one is the *in situ* entrapment of AuNPs in the solid matrix formed by soluble natural polymers [26,27]; another is the direct immobilization of AuNPs on the surface of insoluble natural polymers (i.e., plant fibers) [28,29]. Comparatively, the latter is preferred and promising because the resultant materials exhibit relatively higher activity, because the loaded AuNPs can contact with the reactants more easily, and the complex mass-transfer process needed for the entrapment structure can be avoided [29]. Thus, the development of the eco-friendly catalytic materials derived from natural plant fibers and AuNPs through a facile and mild approach is highly desirable.

Kapok fiber (KF) is a kind of natural, renewable, abundant and low-cost tubular plant fiber with the outer diameter of 15–25 μm and wall thickness of 0.5–2 μm. KF has the advantages including low density, good buoyancy, huge hollowness and better surface activity [30]. The KF fiber is insoluble, and can be easily separated or recovered from liquid system [31,32]. These unique advantages of KF render it potential to be used as the supporter of active nanoparticles. However, the existence of waxy coating on KF makes it hydrophobic and difficult to be dispersed in aqueous solution, and so the active nanoparticles are difficult to be attached on the KF. For improve this, KF was usually coated with polyacrylonitrile through a chemical polymerization reaction [33]. The introduced polyacrylonitrile may enhance the bonding capability of KF to metal ions and is favorable to the attachment of nanoparticles, but the usage of toxic chemicals, modifiers as well as complex chemical reaction is required. Therefore, the design of KF-based catalytic materials through a physical, mild and green approach becomes the hot subject of great interests in the current world that the greening of materials and their preparation methods are highly concerned.

The surface of pretreated KF is negatively charged, and so it is difficult to attract the negatively charged matters. Chitosan (CTS), derived from the second most naturally abundant polysaccharide chitin, is a natural basic polysaccharide with plentiful $-NH_2$ groups [34]. It is renewable, biocompatible, not-toxic and low-cost, and is the fine matrix to produce eco-friendly materials. The positively charged CTS may be easily coated on the surface of KF by a very simple soaking process, and the surface properties of KF can be improved. The CTS-coated KF can combine with the negatively charged nanoparticles with no need of any other chemicals to form a stable nanocomposite.

Based on above description and our previous work [35,36], we employed a facile and efficient non-covalent self-assembly approach to immobilize AuNPs onto KF and carboxylated KF (CKF) to prepare KF-based catalytic materials. The structure and morphologies of the nanocomposite were characterized by UV–visible spectroscopy (UV–*vis*), X-ray diffraction (XRD), scanning electron microscope (SEM) and transmission electron microscope (TEkM), and the catalytic activity was systematically evaluated. In addition, the hydrogen production capability along with the catalytic decoloration of CR dye was evaluated.

2. Experimental

2.1. Materials

Kapok fiber (KF) was purchased from Shanghai Pan–Da Co., Ltd., China. $NaClO_2$ (chemically pure) was provided by Beijing Hua-Wei Chemical Reagent Co., China. Acetic acid (HOAc, Analytical grade) was received from Shanghai Chemical Reagent Factory, Shanghai, China. Chitosan (CTS) with the deacetylation degree (DD) of 90% and molecular weight of 600 kDa was from Yuhuan Ocean Biology Company (Zhejiang, China). Chloroauric acid ($HAuCl_4{\cdot}4H_2O$), sodium borohydride ($NaBH_4$) and chloroacetic acid ($ClCH_2COOH$) were purchased from Sinopharm Chemical Reagent Co., Ltd. (Shanghai, China), and used as received. Congo Red (CR) was purchased from Alfa Aesar and used without further purification. All other reagents are of analytical grade and all solutions were prepared with ultrapure water.

2.2. Immobilization of AuNPs onto KF and CKF

AuNPs were prepared according to the following procedure: 10 mL of the aqueous solution of $HAuCl_4{\cdot}4H_2O$ (1%, *m/v*) was added to 900 mL of ultrapure water in a beaker. Then, 20 mL of the aqueous solution of sodium citrate (1 wt%) was added. After stirred for 5 min, 10 mL of the freshly prepared $NaBH_4$ solution (0.075 wt%) was rapidly added, and the purple-red solution was obtained and cured for 2 h. The concentration of AuNPs in the solution is 0.3129 mmol/L.

Kapok fiber (KF) was pretreated with $NaClO_2$ solution to remove the waxy coating and create a hydrophilic surface as described previously [35,36]. In order to introduce carboxyl groups, the pretreated KF was modified with $ClCH_2COOH$. Typically, 1.0 g of the pretreated KF was dispersed in ultrapure water, and then 0.5 g of $ClCH_2COOH$ was added. Then, the pH values of the reaction system was adjusted to 10 using 1 mol/L of NaOH solution, and the modification reaction was conducted at 60 °C for 2 h. The carboxylated KF (CKF) was separated by suction filtration, and washed with ultrapure water for 5 times to remove the undesired impurities.

The AuNPs can be immobilized on the pretreated KF and CKF in the presence of CTS. Typically, 1.0 g of pretreated KF or CKF was soaked in 200 mL of 0.1 wt% CTS solution (using 1 wt% HOAc solution as the solvents), and the mixture was continuously stirred for 24 h to achieve a saturated and homogeneous adsorption of CTS on the surface of KF. The mixture was separated by suction filtration, and successively washed with 50 mL of 1 wt% aqueous solution of HOAc and ultrapure water for 3 times, respectively. Then, the solution containing AuNPs was gradually added to CTS-coated KF or CKF under continuous stirring, and the addition was stopped when the color of the mixture solution does not fade further (the adsorption was saturated). The added volume of AuNPs solution is 350 mL for KF and 430 mL for CKF, and the calculated loading amount of AuNPs is 2.16 wt% for KF (denoted as KF/CTS/AuNPs) and 2.65 wt% for CKF (denoted as CKF/CTS/AuNPs).

For a comparison, the solution of AuNPs was directly mixed with the KF or CKF without adding CTS, and it was found that the KF or CKF do not adsorb AuNPs. This provides direct evidence that CTS is a key to achieve the immobilization of AuNPs onto KF or CKF. The resultant sample was denoted as KF/AuNPs.

2.3. Evaluation of catalytic activity and recovery capability

0.03 g Of the KF/AuNPs, KF/CTS/AuNPs and CKF/CTS/AuNPs nanocomposites were added into 100 mL of the CR solution (20 mg/L) with and without 0.0568 g of $NaBH_4$. After set time intervals, the nanocomposites were instantly separated from the

solution by suction filtering through a filter (0.45 μm), and the UV–*vis* spectra of the solution were scanned at 25 °C in a range of 300–800 nm and the absorbance was determined at 504 nm using a quartz cell (1 cm path length). The change of absorbance was used as a criterion to evaluate the reduction efficiency. For evaluating the attachment stability of AuNPs, the KF/CTS/AuNPs and CKF/CTS/AuNPs nanocomposites were treated by ultrasonication and 1 mol/L HCl solution for 20 min, respectively. The catalytic properties of the treated nanocomposites were evaluated according to the above similar procedure.

The used CKF/CTS/AuNPs nanocomposites were recycled by suction filtration, washed with distilled water for three times, and then reuse to catalytic reduction of CR dye as the similar procedure described above. The recovery process was repeated for 10 cycles, and the change of decoloration efficiency for CR solution (20 mg/L) within 3 min was used to indicate the recovery capability of the nanocomposite.

2.4. Calculation of reduction rate constants

The reduction rate of dyes, catalyzed by the nanocomposites, was calculated using the following equation.

$$-\ln(C/C_0) = K_{obs}t \quad (1)$$

where C (mg/L) is the concentration of dye at time t, C_0 (mg/L) is the initial concentration of dye, and K_{obs} is the first order rate constant [37].

2.5. Capacity of hydrogen production

Along with the catalytic decoloration of CR solution with $NaBH_4$, hydrogen was simultaneously produced and can be collected as a fuel. The volume of hydrogen was used as a criterion to evaluate the production capability of hydrogen during the reduction process of CR. Typically, 0.3 g of the KF/CTS/AuNPs and CKF/CTS/AuNPs nanocomposites were added into 1000 mL of the CR solution (20 mg/L) with 15 mmol/L of $NaBH_4$. The generated hydrogen in this process was collected by drainage method at set time intervals, and the volume was measured.

2.6. Characterizations

UV–*vis* spectra were determined using a UV–*vis* spectrophotometer (SPECORD 200, Analytik Jera AG). XRD patterns were collected on a X'pert PRO X-ray power diffractometer (PAN analytical Co., Netherlands) using Cu Kα radiation of 1.5406 Å (40 kV, 30 mA). The surface elemental analysis was conducted using an Energy Dispersive Analysis System of X-ray (EDS) (GENESIS, EDAX). The surface morphology was observed using a field emission scanning electron microscope (FESEM, JSM-6701F, JEOL) after coating the samples with gold film. The TEM images were taken using a JEM-2010 high-resolution transmission electron microscope (JEOL, Tokyo, Japan) at an acceleration voltage of 200 kV, and the sample was ultrasonically dispersed in anhydrous ethanol and dropped onto a microgrid before observation.

3. Results and discussion

3.1. Preparation of KF/CTS/AuNPs nanocomposites

The sodium citrate-stabilized AuNPs were successfully prepared using $HAuCl_4{\cdot}4H_2O$ as the precursor and $NaBH_4$ as the reductant. The formation of AuNPs can be confirmed by the surface plasmon resonance peak at 520 nm observed in UV–*vis* spectra (Fig. 1) [38]. The Zeta potential of the solution of AuNPs is −23.4 ± 0.8 mV, and the Zeta potentials of KF, CKF, KF/CTS and CKF/CTS are −28.4 ± 1.8, −41.5 ± 2.1, +11.8 ± 1.4 mV and +12.6 ± 1.2 mV, respectively. Thus, the negatively charged AuNPs are difficult to be attached onto KF or CKF due to the electrostatic repulsion resulting from the same charges. Whereas, the CTS-coated KF or CKF may rapidly attract AuNPs and immoblize them on the surface due to the electrostatic interaction, which acts as the main driving force for the immobilization of AuNPs onto KF or CKF (Fig. 2). From the UV–*vis* spectra of KF/CTS/AuNPs and CKF/CTS/AuNPs, the absorbance peak at 533 nm was clearly observed, which confirmed that the AuNPs were successfully attached on the surface of CTS-coated KF and CKF as expected (Fig. 1). This result can also be intuitively demonstrated in the experiment process that the purple-red solution of AuNPs become colorless when adding the solution into CTS-coated KF or CKF.

3.2. XRD analysis

The attachment of AuNPs on the surface of CTS-coated KF or CKF can also be confirmed by XRD analysis (Fig. 3). As can be seen, the characteristic diffraction peaks of KF appeared at 2θ = 15.78°, 22.62° and 34.96°, which correspond to the (110), (200) and (004) crystallographic planes, respectively [39,40]. The XRD curve of KF have no obvious change after directly mixed it with AuNPs (KF/AuNPs), and no the diffraction peaks of AuNPs can be observed. This indicates that AuNPs fail to be directly attached on KF. However, the characteristic diffraction peaks of AuNPs at 2θ = 38.56° (111) and 44.67° (200) [41] (JCPDF No. 04-0784) appeared in the XRD curves of KF/CTS/AuNPs and CKF/CTS/AuNPs. This indicates that AuNPs was attached on KF and CKF when using CTS as a "bridge", and CTS is essential to the self-assembly process. It can also be observed that the intensity of diffraction peaks of AuNPs for CKF/CTS/AuNPs is stronger than that of KF/CTS/AuNPs, indicating that the carboxylation of KF is more favorable to the attachment of AuNPs in contrast to KF. The XRD result is consistent with the UV–*vis* analysis (Fig. 1). According to the EDS results (figure is not shown), it can be found that the loading amounts of AuNPs on KF and CKF are about 2.07 ± 0.07 wt% (n = 6) and 2.52 ± 0.08 wt% (n = 6), respectively, which is close to the values calculated by the volume of used AuNPs solutions.

3.3. SEM and TEM analyses

The surface appearances of KF, KF/AuNPs, KF/CTS/AuNPs, CKF/CTS/AuNPs were observed using FESEM, and the AuNPs on the surface of KF was observed using TEM (Fig. 4). It can be clearly

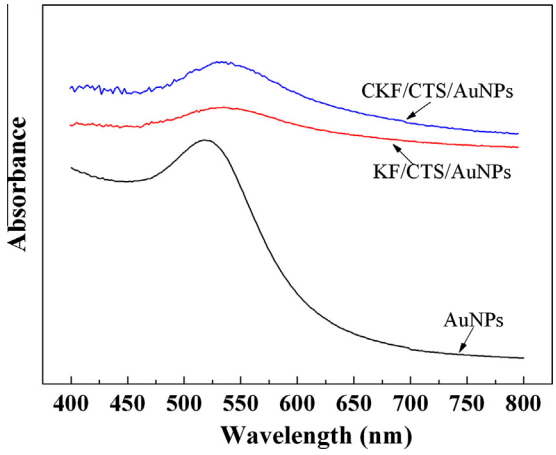

Fig. 1. The UV–*vis* spectra of AuNPs, KF/CTS/AuNPs and CKF/CTS/AuNPs.

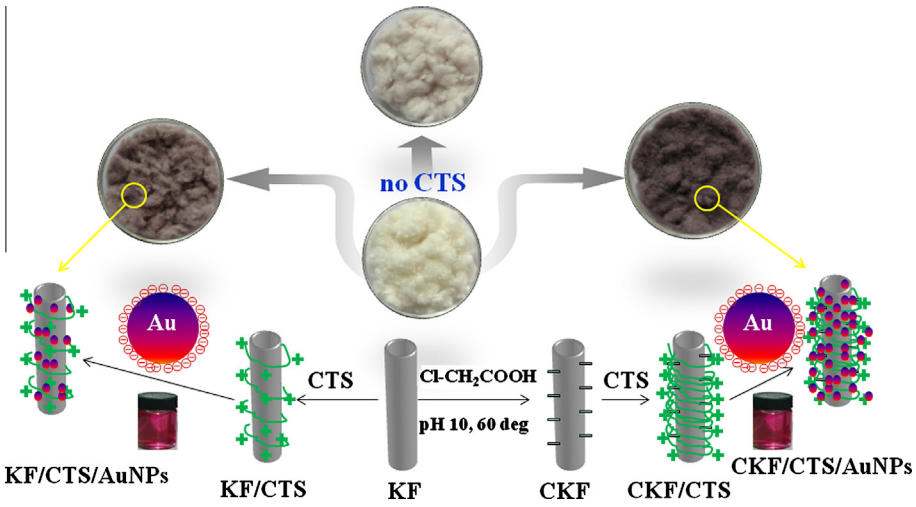

Fig. 2. Scheme for the non-covalent self-assembly mechanism of KF/CTS/AuNPs and CKF/CTS/AuNPs.

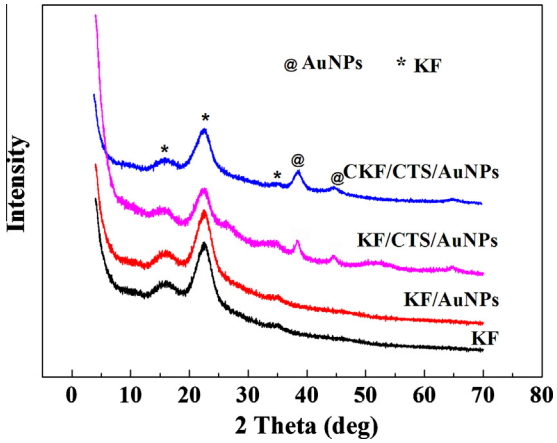

Fig. 3. XRD diffraction patterns of (a) pretreated KF, (b) CKF, KF/CTS/AuNPs and (c) CKF/CTS/AuNPs.

observed that KF shows a smooth surface (Fig. 4a). After carboxylation, the surface of KF becomes relatively rough with subtle textures (Fig. 4b), indicating that chloroacetic acid was reacted with KF, which is consistent with the change of Zeta potential (from −28.4 ± 1.8 to −41.5 ± 2.1 mV). The negatively charged surface can be easily coated with CTS, and the negatively charged AuNPs can be adsorbed onto the CTS-coated KF or CKF. Correspondingly, the surface of the KF/CTS/AuNPs and CKF/CTS/AuNPs becomes rough and many wrinkles were observed (Fig. 4c and d), which implies that the CTS coating was formed on the surface of KF. The AuNPs can be observed from the TEM images of KF/CTS/AuNPs and CKF/CTS/AuNPs (Fig. 4e and f), and the existence of AuNPs can be confirmed by the appearance of characteristic peak of Au in the energy-dispersive X-ray spectroscopy (EDX) of CKF/CTS/AuNPs (Supporting Information, Fig. S1). It was observed that the AuNPs exhibit a very well dispersion and uniform distribution on the surface of KF without obvious aggregations among particles. The AuNPs with the size distribution of 3–5 nm were tightly anchored on the KF surface to form a better nanocomposite structure. By contrast, the distribution of nanoparticles is relatively denser on the surface of CKF/CTS/AuNPs than that of KF/CTS/AuNPs, indicating that the carboxylation of KF is favorable to the attachment of AuNPs.

3.4. Catalytic activity

As shown in Fig. 5, the addition of $NaBH_4$ to the solutions of CR dye does not cause any appreciable change in the absorbance of solution and no hydrogen generated in the absence of the catalyst, indicating that BH_4^- ions cannot reduce the CR dyes. After adding KF or KF/AuNPs into the solution, the absorbance was slightly decreased, but no obvious decoloration of CR dye was observed. This indicates that the KF or KF/AuNPs have no additional catalytic action to the reducing decoloration of CR dye, and only weaker adsorption action of KF or KF/AuNPs for CR dye was occurred. However, when the KF/CTS/AuNPs and CKF/CTS/AuNPs nanocomposites were added to the CR solution containing BH_4^- ions, the absorbance was rapidly decreased until it is close to zero, and the color of solution almost becomes colorless within 3 min (Fig. 6). Fig. 5b shows the fitting curves of $\ln(C/C_0)$ versus t, and the rate constant K_{obs} can be calculated. The catalytic reduction rate constants are 0.0171 s^{-1} (for KF/CTS/AuNPs), 0.0229 s^{-1} (CKF/CTS/AuNPs), 0.0223 s^{-1} (CKF/CTS/AuNPs after sonication) and 0.0225 s^{-1} (CKF/CTS/AuNPs after acid treatment). The reduction rate of CR solution catalyzed by CKF/CTS/AuNPs is faster than that of KF/CTS/AuNPs, indicating that the increase of loading amount of Au^0 in the nanocomposite is favorable to improve its catalytic rate. Moreover, the nanocomposite still has excellent catalytic activity after treated with ultrasonnication and 1 mol/L HCl solution for 20 min (Figs. 5 and 6), and the catalytic reduction rate constants of CKF/CTS/AuNPs are slightly decreased from 0.0229 s^{-1} to 0.0223 s^{-1} (after sonication) and 0.0225 s^{-1} (after acid treatment). This also proved that the nanocomposite has satisfactory stability besides excellent activity. Table 1 listed the catalytic decoloration efficiency of different catalysts for CR dye. By contrast, the catalytic reduction using CKF/CTS/AuNPs as the catalyst can decolor CR solution within shorter 3 min, which reflects the relatively higher decoloration efficiency.

It can be noticed from Fig. 5 that the absorbance of the CR at 350 nm was shifted to 360 nm along with the disappearance of the absorbance peak at 540 nm, which implies that the azo CR molecules were reduced to form a new product. Fig. 7 illustrates the proposed catalytic reduction mechanism, it can be seen that the AuNPs trigger the catalytic reduction by relaying electron from the BH_4^- donor to the acceptor molecules of CR dye, and the KF/CTS/AuNPs or CKF/CTS/AuNPs can receive and convey electrons to the dyes more effectively [48,49]. As a result, the azo double —N=N— bonds were reduced as the —N—N— bonds, and the red CR dye was faded (Figs. 6 and 7).

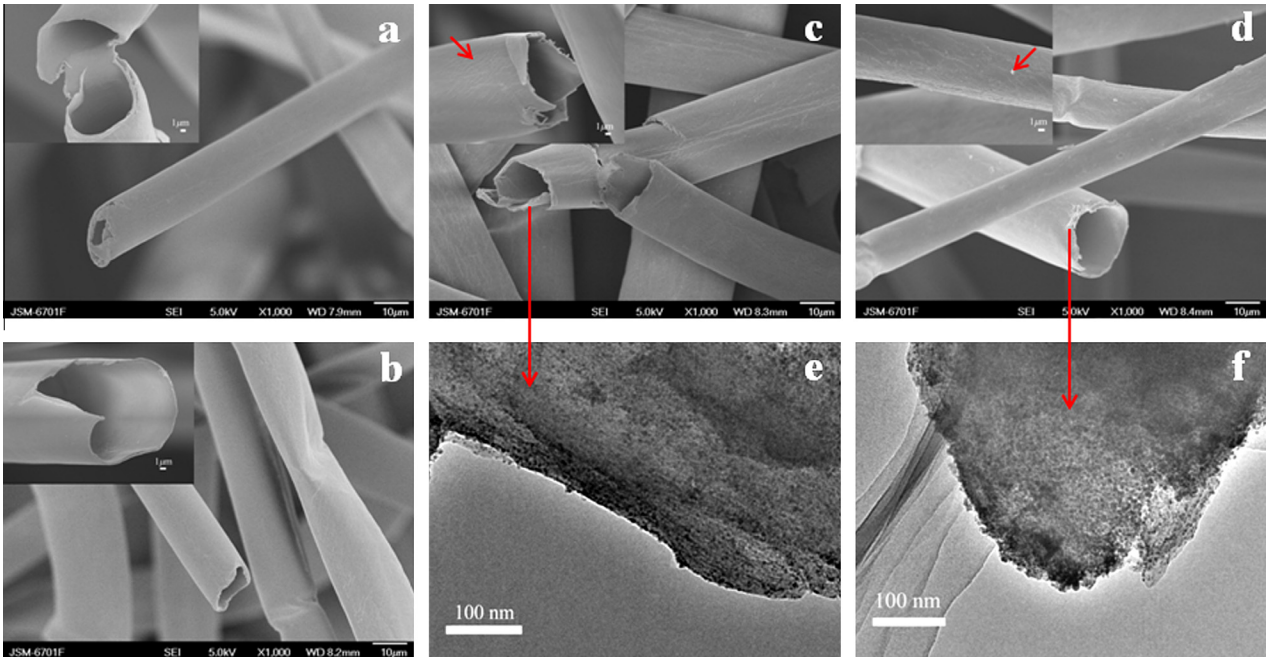

Fig. 4. SEM micrographs of (a) KF, (b) CKF, (c) KF/CTS/AuNPs and (d) CKF/CTS/AuNPs, and the inset is the corresponding magnification images; TEM image of (e) KF/CTS/AuNPs and (f) CKF/CTS/AuNPs.

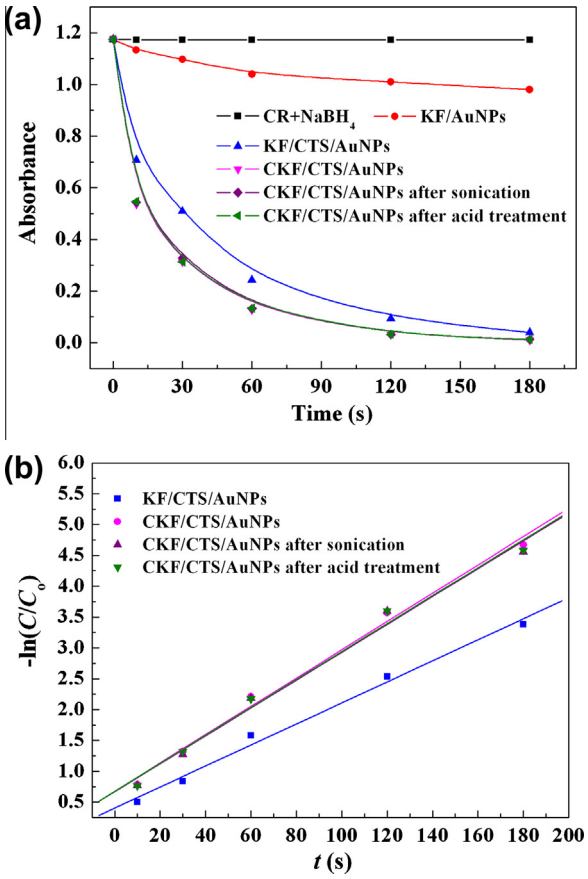

Fig. 5. (a) Catalytic kinetic curves of KF/AuNPs, KF/CTS/AuNPs and CKF/CTS/AuNPs before and after sonication and acid treatment (1 mol/L HCl solution, 20 min) for the reduction of CR solution (initial CR concentration, 20 mg/L; initial $NaBH_4$ concentration, 15 mmol/L; catalyst dosage, 0.3 g/L); (b) linear relationship of $-\ln(C/C_0)$ as a function of time t.

Besides the catalytic activity, the reusability of the nanocomposite as a catalyst is also important to its practical application. Fig. 8 shows the decoloration percentage (%) of CR solution within 3 min after repeated for 10 cycles. It can be observed that the decoloration percentage has no obvious decrease, and 92.6% of the initial decoloration percentage was achieved after recovered for 9 times. This indicates that the nanocomposite can be used as recyclable catalysis materials for decoloraiton applications.

3.5. Capacity of hydrogen production

As shown in Fig. 9, the reduction of CR molecules and the oxidation of BH_4^- ions generated hydrogen. The production of hydrogen from $NaBH_4$ by a catalytic oxidation–reduction reaction was reported and the corresponding mechanism was explored [50,51]. In order to improve the hydrogen production efficiency, the addition of additional chemical agents such as NaOH, methanol, ethanol is required [50,51]. In our work, the dye molecules were acted as the acceptor of electrons, and so the NaBH4 was rapidly transformed as hydrogen gas and simultaneously the dye molecules were decolored (Fig. 7). The advantages of this process is that, (i) the overflow of hydrogen gas from the surface of the nanocomposite to the solution causes the convection of the solution and keeps the effective transfer of dye solution to the nanocomposite; (ii) the generated hydrogen gas can be collected and reused as the clean fuel. As shown in Fig. 9, the output amount of hydrogen gas rapidly increased with prolonging the reaction time, until a constant value was reached. The maximum hydrogen gas production amount is about 430 mL for each liter of CR dye wastewater (20 mg/L). From this point of view, using the eco-friendly KF/CTS/AuNPs and CKF/CTS/AuNPs as catalysts, we can produce hydrogen energy by consuming CR dye waste water, and this idea will be promising and contributory to alleviate environmental and energy problems.

4. Conclusions

The AuNPs-decorated KF nanocomposites were successfully prepared by a simple, green and mild non-covalent approach using

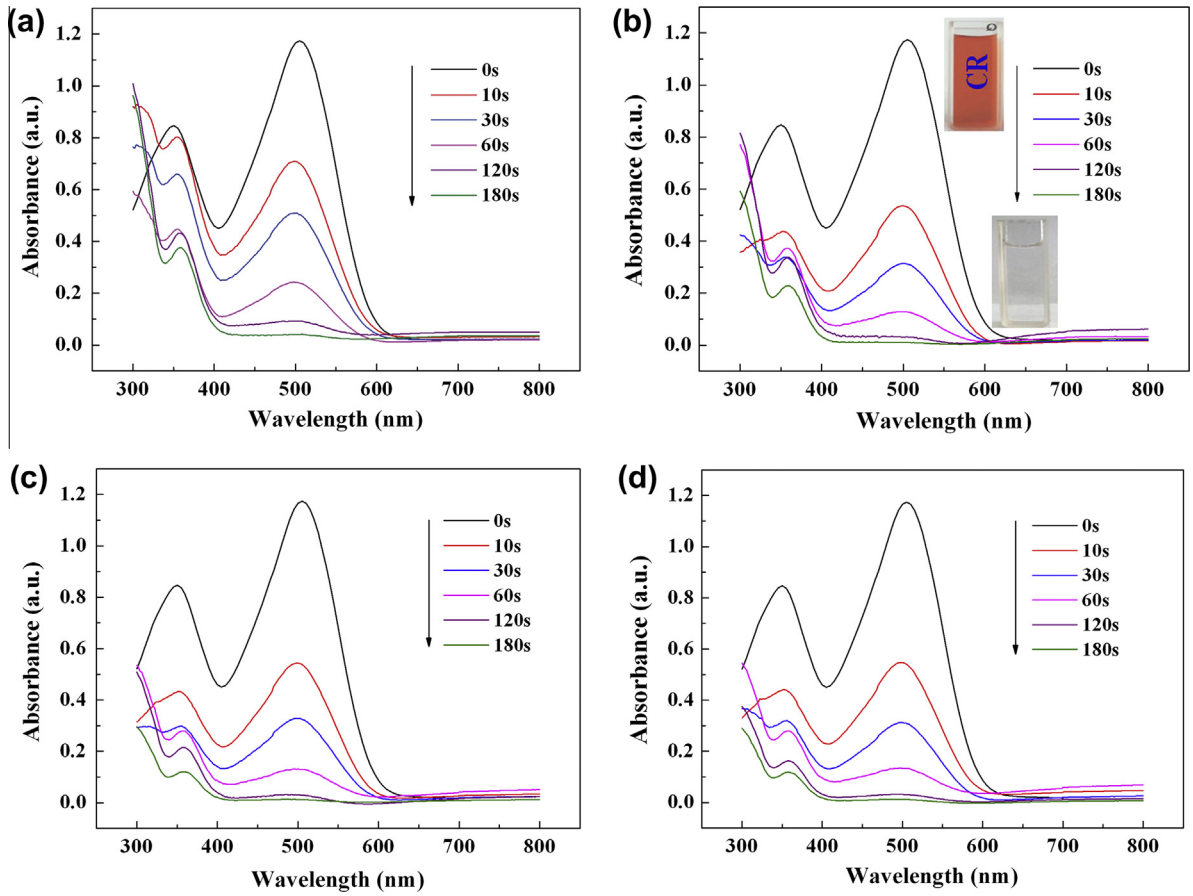

Fig. 6. Time dependent UV–*vis* absorption spectra for the catalytic reduction of CR by $NaBH_4$ in the presence of KF/CTS/AuNPs (a), CKF/CTS/AuNPs before (b), and after sonication (c) and acid treatment by 1 mol/L HCl solution (d).

Table 1
Comparison of decoloration efficiency for CR dye using various catalysts.

Catalysts	Dosage (g/L)	Initial conc. (mg/L)	Decoloration time	Refs.
Chitosan/nano-CdS	1.5	20	180 min	[42]
TiO_2	1.0	55	480 min	[43]
UV/H_2O_2	1.7	50	60 min	[44]
Fe modified Y zeolite	1.5	–	10–45 min	[45]
WO_3–TiO_2/activated carbon	10	10	120	[46]
Ba—Cd—Sr—Ti Doped Fe_3O_4	1	25	2 h	[47]
CKF/CTS/AuNPs	0.3	20	3 min	This work

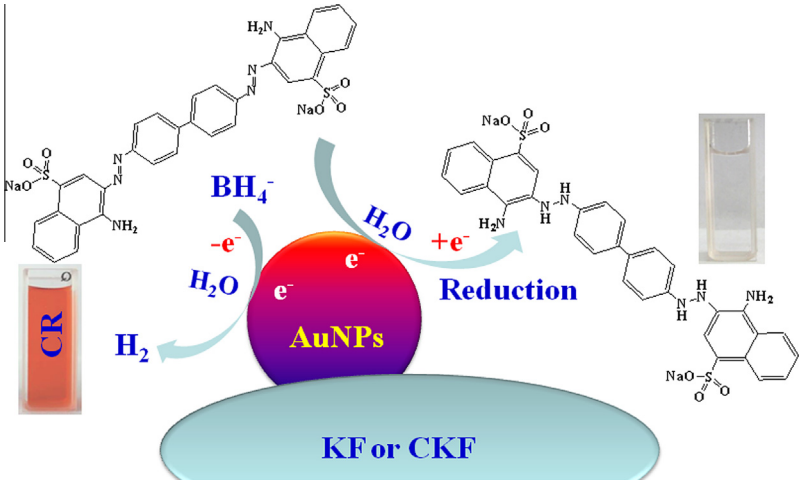

Fig. 7. Proposed mechanisms for the catalytic reduction of CR dye by $NaBH_4$ using KF/CTS/AuNPs or CKF/CTS/AuNPs as the catalysts.

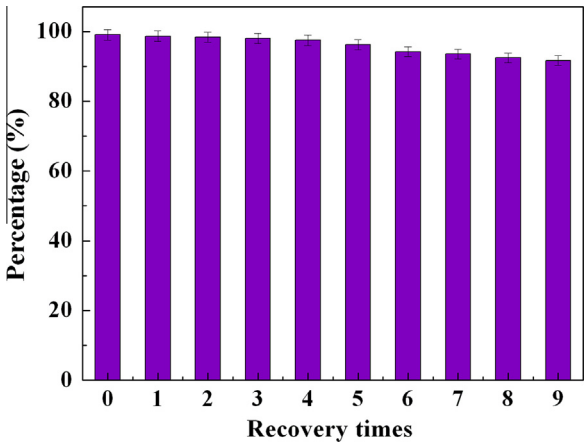

Fig. 8. The catalytic efficiency of the CKF/CTS/AuNPs nanocomposite after repeated 10 times.

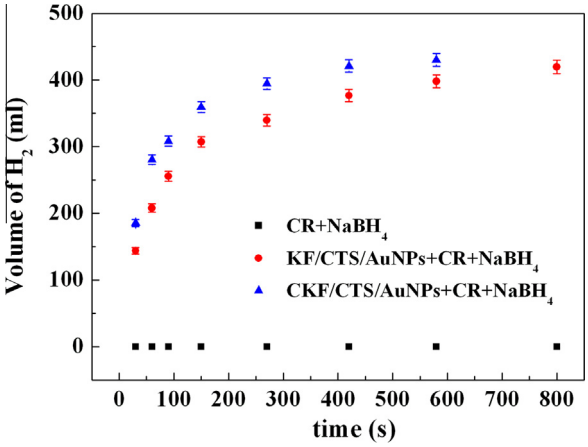

Fig. 9. The variation of hydrogen production volume against time (initial CR dye concentration, 20 mg/L; initial volume of CR solution, 1 L; initial $NaBH_4$ concentration, 15 mmol/L; initial dosage of catalyst, 0.3 g/L).

natural KF as the matrix and CTS as the "bridge". In this process, the negatively charged AuNPs can be easily immobilized on KF or CKF through electrostatic interaction in the presence of CTS as a "double side tape", and the AuNPs exhibited a well-dispersed distribution on the KF or CKF matrix. The as-prepared nanocomposites exhibited excellent catalytic performance for the reducing decoloration of CR dye by $NaBH_4$ in aqueous solution, and the solution of CR dye (20 mg/L) can be rapidly decolored with 3 min at a low dosage of 0.3 g/L. Along with the decoloration of CR dye, the hydrogen gas was generated and collected as a clean fuel, and the maximum yield reached 430 mL/L CR solution (20 mg/L). More importantly, the nanocomposite based on plant fiber can be easily separated from the liquid system, which is favorable for the recycle of the materials. After being sonicated and acid treated, the nanocomposite still retain better catalytic activities, and the activity only decreased a little after reuse for 10 cycles. This indicates that the nanocomposite has better stability and reusability. As a whole, the development of the nanocomposites based on natural plant fiber KF by a facile and green method, and their applications for decoloration of dye wastewater and the simultaneous H_2 production opened a new avenue to utilize natural resources and alleviate the experimental problems.

Acknowledgements

This work is supported by the National Natural Science Foundation of China (No. 21107116) and the "863" Project of the Ministry of Science and Technology, China (No. 2013AA031403).

Appendix A. Supplementary material

Supplementary data associated with this article can be found, in the online version, at http://dx.doi.org/10.1016/j.cej.2013.10.044.

References

[1] E.C. Dreaden, A.M. Alkilany, X.H. Huang, C.J. Murphy, M.A. El-Sayed, The golden age: gold nanoparticles for biomedicine, Chem. Soc. Rev. 41 (2012) 2740–2779.
[2] P. Joshi, S. Chakraborti, J.E. Ramirez-Vick, Z.A. Ansari, V. Shanker, P. Chakrabarti, S.P. Singh, The anticancer activity of chloroquine-gold nanoparticles against MCF-7 breast cancer cells, Colloids Surf. B: Biointerf. 95 (2012) 195–200.
[3] C. Gutiérrez-Sánchez, M. Pita, C. Vaz-Domínguez, S. Shleev, A.L. De Lacey, Gold nanoparticles as electronic bridges for laccase-based biocathodes, J. Am. Chem. Soc. 134 (2012) 17212–17220.
[4] Y.X. Li, J.T. Cox, B. Zhang, Electrochemical responses and electrocatalysis at single Au nanoparticles, J. Am. Chem. Soc. 132 (2010) 3047–3054.
[5] K. Saha, S.S. Agasti, C. Kim, X.N. Li, V.M. Rotello, Gold nanoparticles in chemical and biological sensing, Chem. Rev. 112 (2012) 2739–2779.
[6] X.W. Liu, F.Y. Wang, F. Zhen, J.R. Huang, *In situ* growth of Au nanoparticles on the surfaces of Cu_2O nanocubes for chemical sensors with enhanced performance, RSC Adv. 2 (2012) 7647–7651.
[7] C.O. Baker, B. Shedd, R.J. Tseng, A.A. Martinez-Morales, C.S. Ozkan, M. Ozkan, Y. Yang, R.B. Kaner, Size control of gold nanoparticles grown on polyaniline nanofibers for bistable memory devices, ACS Nano 5 (2011) 3469–3474.
[8] M.S. Strozyk, M. Chanana, I. Pastoriza-Santos, J. Pérez-Juste, L.M. Liz-Marzán, Stimuli-responsive materials: protein/polymer-based dual-responsive gold nanoparticles with pH-dependent thermal sensitivity, Adv. Funct. Mater. 22 (2012) 1322.
[9] D.H. Wang, D.Y. Kim, K.W. Choi, J.H. Seo, S.H. Im, J.H. Park, O.O. Park, A.J. Heeger, Enhancement of donor–acceptor polymer bulk heterojunction solar cell power conversion efficiencies by addition of Au nanoparticles, Angew. Chem. 123 (2011) 5633–5637.
[10] M. Stratakis, H. Garcia, Catalysis by supported gold nanoparticles: beyond aerobic oxidative processes, Chem. Rev. 112 (2012) 4469–4506.
[11] A. Corma, H. Garcia, Supported gold nanoparticles as catalysts for organic reactions, Chem. Soc. Rev. 37 (2008) 2096–2126.
[12] F.B. Lollmahomed, R. Narain, Photochemical approach toward deposition of gold nanoparticles on functionalized carbon nanotubes, Langmuir 27 (2011) 12642–12649.
[13] P. Gobbo, M.C. Biesinger, M.S. Workentin, Facile synthesis of gold nanoparticle (AuNP)–carbon nanotube (CNT) hybrids through an interfacial Michael addition reaction, Chem. Commun. 49 (2013) 2831–2833.
[14] R. Muszynski, B. Seger, P.V. Kamat, Decorating graphene sheets with gold nanoparticles, J. Phys. Chem. C 112 (2008) 5263–5266.
[15] M. Wojnicki, M. Luty-Błocho, J. Grzonka, K. Pacławski, K.J. Kurzydłowski, K. Fitzner, Micro-continuous flow synthesis of gold nanoparticles and integrated deposition on suspended sheets of graphene oxide, Chem. Eng. J. 225 (2013) 597–606.
[16] T. Wu, L. Zhang, J.P. Gao, Y. Liu, C.J. Gao, J. Yan, Fabrication of graphene oxide decorated with Au–Ag alloy nanoparticles and its superior catalytic performance for the reduction of 4-nitrophenol, J. Mater. Chem. A 1 (2013) 7384–7390.
[17] H. Zhu, M.L. Du, M.L. Zou, C.S. Xu, N. Li, Y.Q. Fu, Facile and green synthesis of well-dispersed Au nanoparticles in PAN nanofibers by tea polyphenols, J. Mater. Chem. 22 (2012) 9301–9307.
[18] E. Lam, S. Hrapovic, E. Majid, J.H. Chonga, J.H.T. Luong, Catalysis using gold nanoparticles decorated on nanocrystalline cellulose, Nanoscale 4 (2012) 997–1002.
[19] H. Koga, E. Tokunaga, M. Hidaka, Y. Umemura, T. Saito, A. Isogai, T. Kitaoka, Topochemical synthesis and catalysis of metal nanoparticles exposed on crystalline cellulose nanofibersw, Chem. Commun. 46 (2010) 8567–8569.
[20] H. Zhu, M.L. Du, M.L. Zou, C.S. Xu, Y.Q. Fu, Green synthesis of Au nanoparticles immobilized on halloysite nanotubes for surface-enhanced Raman scattering substrates, Dalton Trans. 41 (2012) 10465–10471.
[21] M. Yadav, T. Akita, N. Tsumoriab, Q. Xu, Strong metal–molecular support interaction (SMMSI): amine-functionalized gold nanoparticles encapsulated in silica nanospheres highly active for catalytic decomposition of formic acid, J. Mater. Chem. 22 (2012) 12582–12586.
[22] A. Boullanger, S. Clément, V. Mendez, S. Daniele, C. Thieuleux, A. Mehdi, SH-functionalized cubic mesostructured silica as a support for small gold nanoparticles, RSC Adv. 3 (2013) 725–728.
[23] Y.J. Chen, G.H. Tian, K. Pan, C.G. Tian, J. Zhou, W. Zhou, Z.Y. Ren, H.G. Fu, Green synthesis of Au nanoparticles immobilized on halloysite nanotubes for

surface-enhanced Raman scattering substrates, Dalton Trans. 41 (2012) 1020–1026.
[24] I. Šimkovic, What could be greener than composites made from polysaccharides?, Carbohydr Polym. 74 (2008) 759–762.
[25] X.D. Wu, C.H. Lu, W. Zhang, G.P. Yuan, R. Xiong, X.X. Zhang, A novel reagentless approach for synthesizing cellulose nanocrystals-supported palladium nanoparticles with enhanced catalytic performance, J. Mater. Chem. A 1 (2013) 8645–8652.
[26] S. Saha, A. Pal, S. Kundu, S. Basu, T. Pal, Photochemical green synthesis of calcium-alginate-stabilized Ag and Au nanoparticles and their catalytic application to 4-nitrophenol reduction, Langmuir 26 (2010) 2885–2893.
[27] J. Shan, H. Tenhu, Recent advances in polymer protected gold nanoparticles: synthesis, properties and applications, Chem. Commun. (2007) 4580–4598.
[28] T. Ishida, H. Watanabe, T. Bebeko, T. Akita, M. Haruta, Aerobic oxidation of glucose over gold nanoparticles deposited on cellulose, Appl. Catal. A: Gen. 377 (2010) 42–46.
[29] P. Gomathi, D. Ragupathy, J.H. Choi, J.H. Yeum, S.C. Lee, J.C. Kim, S.H. Lee, H.D. Ghim, Fabrication of novel chitosan nanofiber/gold nanoparticles composite towards improved performance for a cholesterol sensor, Sens. Act. B: Chem. 153 (2011) 44–49.
[30] T.-T. Lim, X.F. Huang, Evaluation of kapok (Ceiba pentandra (L.) Gaertn.) as a natural hollow hydrophobic–oleophilic fibrous sorbent for oil spill cleanup, Chemosphere 66 (2007) 955–963.
[31] M.A. Abdullah, A.U. Rahmah, Z. Man, Physicochemical and sorption characteristics of Malaysian Ceiba pentandra (L.) Gaertn. as a natural oil sorbent, J. Hazard. Mater. 177 (2010) 683–691.
[32] X.F. Huang, T.T. Lim, Performance and mechanism of a hydrophobic–oleophilic kapok filter for oil/water separation, Desalination 190 (2006) 295–307.
[33] H.S. Fan, X.L. Yu, Y.H. Long, X.Y. Zhang, H.F. Xiang, C.T. Duan, N. Zhao, X.L. Zhang, J. Xu, Preparation of kapok–polyacrylonitrile core–shell composite microtube and its application as gold nanoparticles carrier, Appl. Surf. Sci. 258 (2012) 2876–2882.
[34] R.A.A. Muzzarelli, F. Greco, A. Busilacchi, V. Sollazzo, A. Gigante, Chitosan, hyaluronan and chondroitin sulfate in tissue engineering for cartilage regeneration: a review, Carbohydr. Polym. 89 (2012) 723–739.
[35] Y. Liu, J.T. Wang, Y.A. Zheng, A.Q. Wang, Adsorption of methylene blue by Kapok fiber treated by sodium chlorite optimized with response surface methodology, Chem. Eng. J. 184 (2012) 248–255.
[36] Y.A. Zheng, W.B. Wang, D.J. Huang, A.Q. Wang, Kapok fiber oriented-polyaniline nanofibers for efficient Cr(VI) removal, Chem. Eng. J. 191 (2012) 154–161.
[37] G.H. Zhao, J.Z. Wang, Y.F. Li, X. Chen, Y.P. Liu, Enzymes immobilized on superparamagnetic Fe_3O_4@Clays nanocomposites: preparation, characterization, and a new strategy for the regeneration of supports, J. Phys. Chem. C 115 (2011) 6350–6359.
[38] W. Haiss, N.T.K. Thanh, J. Aveyard, D.G. Fernig, Determination of size and concentration of gold nanoparticles from UV−Vis spectra, Anal. Chem. 79 (2007) 4215–4221.
[39] M.S. Islam, S. Hamdan, I. Jusoh, M.R. Rahman, A.S. Ahmed, The effect of alkali pretreatment on mechanical and morphological properties of tropical wood polymer composites, Mater. Design 33 (2012) 419–424.
[40] M. Wada, J. Suciyama, T. Okano, Native celluloses on the basis of two crystalline phase (lα/1β) system, J. Appl. Polym. Sci. 49 (1993) 1491–1496.
[41] X.H. Liu, J. Zhang, X.Z. Guo, S.R. Wang, S.H. Wu, Core–shell α–Fe_2O_3@ SnO_2/Au hybrid structures and their enhanced gas sensing properties, RSC Adv. 2 (2012) 1650–1655.
[42] H.Y. Zhu, R. Jiang, L. Xiao, Y.H. Chang, Y.J. Guan, X.D. Li, G.M. Zeng, Photocatalytic decolorization and degradation of Congo Red on innovative crosslinked chitosan/nano-CdS composite catalyst under visible light irradiation, J. Hazard Mater. 169 (2009) 933–940.
[43] L. Ćurković, D. Ljubas, H. Juretić, Photocatalytic decolorization kinetics of diazo dye Congo Red aqueous solution by UV/TiO_2 nanoparticles, Reac. Kinet. Mech. Cat. 99 (2012) 201–208.
[44] D. Kamel, A. Sihem, C. Halima, S. Tahar, Decolourization process of an azoïque dye (Congo Red) by photochemical methods in homogeneous medium, Desalination 247 (2009) 412–422.
[45] A.K. Kondru, P. Kumar, S. Chand, Catalytic wet peroxide oxidation of azo dye (Congo Red) using modified Y zeolite as catalyst, J. Hazard. Mater. 166 (2009) 342–347.
[46] J.H. Sun, Y.K. Wang, R.X. Sun, S.Y. Dong, Photodegradation of azo dye Congo Red from aqueous solution by the WO_3–TiO_2/activated carbon (AC) photocatalyst under the UV irradiation, Mater. Chem. Phys. 115 (2009) 303–308.
[47] R. Rahimi, A. Tadjarodi, M. Rabbani, H. Kerdari, M. Imani, Preparation, characterization and photocatalytic properties of Ba–Cd–Sr–Ti doped Fe_3O_4 nanohollow spheres on removal of Congo Red under visible-light irradiation, J. Supercond. Nov. Magn. 26 (2013) 219–228.
[48] W. Li, J. Li, W.B. Qiang, J.J. Xu, D.K. Xu, Enzyme-free colorimetric bioassay based on gold nanoparticle-catalyzed dye decolorization, Analyst 138 (2013) 760–766.
[49] U.P. Azad, V. Ganesan, M. Pal, Catalytic reduction of organic dyes at gold nanoparticles impregnated silica materials: influence of functional groups and surfactants, J. Nanopart. Res. 13 (2011) 3951–3959.
[50] S. Galli, M. De Francesco, G. Monteleone, R. Oronzio, A. Pozio, Development of a compact hydrogen generator from sodium borohydride, Int. J. Hydrogen Energy 35 (2010) 7344–7349.
[51] V.R. Fernandes, A.M.F.R. Pinto, C.M. Rangel, Hydrogen production from sodium borohydride in methanol–water mixtures, Int. J. Hydrogen Energy 35 (2010) 9862–9868.